A Dual-Polarized Leaky Lens Antenna for Wideband Focal Plane Arrays

Yurduseven, O.; Llombart Juan, N.; Neto, A.

Important note
To cite this publication, please use the final published version (if applicable).
Please check the document version above.

A Dual-Polarized Leaky Lens Antenna for Wideband Focal Plane Arrays

Ozan Yurduseven, *Student Member, IEEE*, Nuria Llombart Juan, *Senior Member, IEEE*, and Andrea Neto, *Fellow Member, IEEE*

Abstract—This paper presents the design and measurements of a wideband dual polarized leaky lens antenna suitable for tightly spaced focal plane arrays. The antenna is composed of two crossed leaky slots fed by two orthogonal microstrips to realize the dual-polarization operation. The crossed microstrips are fed differentially in order to couple the radiation into the slots. The slots are then coupled to a dielectric lens to achieve directive patterns suited for feeding large Focal distance to Diameter ratio reflectors. In this paper, the proposed leaky lens antenna is optimized to achieve high aperture efficiency with clean symmetric patterns in both polarizations exceeding an octave bandwidth. The concept is validated by the measurements of the primary fields inside the lens and with GRASP simulations of the focal plane array.

Index Terms—Broadband antennas, dual-polarization, leaky lens antennas.

Fig. 1. Schematic of the FPA design with its design parameters.

I. INTRODUCTION

APPLICATIONS in imaging, radio astronomy, and space science typically require antennas that are able to provide multibeam solutions with large operational bandwidths. Many of the instruments used for these kinds of applications are based on antenna arrays located on the focal plane of a large reflector. Future scientific instruments operating in the submillimeter band of the spectrum are envisioned to have large format focal plane arrays (FPA) that are based on a single beam per feed and tight sampling and are coupled to reflector systems with large Focal distance to Diameter ratio (F/D) ratios (>3) [1], [2].

For microwave frequencies, several wide bandwidth single reflector feeds such as ridged horn antennas [3], Eleven antenna [4], a coherently fed connected array of slots coupled to silicon lenses [5], and studies with optimized lens profiles in [6] and [7] have been proposed with nearly stable frequency patterns coupled to small F/D ratios. Single feed solutions, however, are optimized for efficient reflector illumination over wide bandwidths. As a consequence, such feed solutions

are typically characterized by a low taper efficiency of the reflector feed. Instead, for focal plane arrays, Vivaldi [8], [9], corrugated horn [11]–[16] or spline horn antennas [17], [18] are the most widely used antennas at low frequencies. These later antennas can provide relatively low sidelobes and cross-polarization levels at a moderate bandwidth with higher taper efficiencies than the single feed systems. When the instruments require tightly spaced FPAs for full sampling of the focal field, the taper efficiency of the feed antennas becomes particularly critical for the overall system performance, as it affects the spillover from the reflector [19]. The aim of this work is to design a tightly sampled wideband dual-polarized FPA feed with high aperture efficiency that could be used at high frequencies where large F/D ratios are typically preferred.

Lens antennas are widely used in the submillimeter band as they allow the integration of the antenna and detector on the same chip. Space instruments based on cryogenic power detectors often use focal plane arrays based on dielectric lenses. In [20], an astronomical instrument based on about 25-k FPA elements based on kinetic inductance detector (KID) slot antennas coupled to silicon lenses has been developed. Achieving the mentioned number of array elements is a challenging target for any kind of horn antennas with the fabrication techniques available nowadays. In the literature, the most commonly used lens feed is a double slot antenna, which typically operates in a bandwidth much less than one octave and with single polarization [21]. Other slot-based lens feeds have been proposed to improve the impedance bandwidth [22]–[26], typically at the cost of the quality of the patterns. Sinuous antennas and spiral have been also proposed

TABLE I

REFLECTOR FEEDS FOR FPA APPLICATIONS

Antenna type	Aperture size	Frequency range	Aperture efficiency	PFL*	Polarization	Directivity (Central freq)	X-pol
Corrugated horn [11] [12]	$5\lambda_0$ $3.7\lambda_0$	$1:1.5$ $1:1.6$	Between 38%-53% Between 38%-58%	No No	Linear**	≈ 20.5dB ≈ 18.66dB	< -30dB < -20dB
Spline horn [17]	$9.5\lambda_0$	$1:1.16$	Between 49%-54%	No	Linear	≈ 26.4dB	< -28dB
Double slot antenna [21] (with a synthesized elliptical lens)	$11.23\lambda_0$	$1:1.15$	Between 60%-75%	Yes	Linear	≈ 30dB	< -20dB
X-slot antenna [22], [23] (with an elliptical lens)	$11.33\lambda_0$	$1:2$	Between 40%-50%	Yes	Linear	≈ 28.7dB	< -12dB
Sinuous antenna [27] (with an ext. hemispherical lens)	$6.35\lambda_0$	$1:4$ (@12GHz, @24GHz)	Between 39%-50% (Estimated) (50%, 43%) (Estimated)	Yes***	Dual	≈ 22dB	< -17dB
This work (with an ext. hemispherical lens)	$10.66\lambda_0$	$1:2.5$ $1:5.25$	Over 60% Over 50%	Yes	Dual	≈ 28.7dB	< -12dB

λ_0: Free-space wavelength at the central frequency, f_0
*PFL: Planar feeding lines
** Dual polarized version may also be possible
*** Beam distortion due to the radiation of planar feeding lines unless the lines are extremely tiny in terms of wavelength

in [27]–[29] to provide wideband solutions. The main limitation of these antennas is the difficulty to integrate them with planar transmission lines [29]. A new lens feed concept was proposed in [30], which is able to operate at multioctave bandwidths. This antenna consists of a leaky-wave slot kept at an electrically small distance from the dielectric lens in order to improve the lens illumination. Recently, the combination of this leaky lens antenna with KIDs has been proved to give a nearly independent frequency response from 350 GHz up to 1.2 THz [31]. However, such antenna had very low aperture efficiency, being suitable only for single feed systems.

In this paper, we present the optimization of a tightly spaced FPA based on such a concept, see Fig. 1. Improving on the antenna concept presented in [30], we propose a dual-polarized extension that is able to provide high feed aperture efficiency over an octave bandwidth. It consists of two orthogonal slots coupled to the two independent microstrips, which can be easily integrated to differential receivers or KIDs. To the best of our knowledge, the proposed leaky lens antenna is the only practical wideband dual-polarization solution that can be integrated to planar feeding lines on the same chip presently available at high frequencies.

This paper is organized as follows. In Section II, we briefly mention the state-of-the-art solutions proposed for tightly spaced FPAs and compare their performances. In Section III, we introduce the antenna concept and explain the slot excitation mechanism. This section mainly focuses on a parametric study to optimize the antenna radiation in the presence of a semi-infinite silicon stratification to maximize the feed taper efficiency on the lens aperture. In Section IV, we show the experimental validation of the radiation patterns inside semi-infinite silicon. Section V focuses on FPA lens optimization, where we show the performance of a leaky lens antenna array together with the reflector illumination. Finally, the conclusions are given in Section VI.

II. STATE-OF-THE-ART IN TIGHTLY SPACED FPAs

In this section, we provide a detailed summary of the different antenna geometries that could be used in wideband and tightly spaced FPAs. Table I gives the summary of the operational bandwidth and aperture efficiency values, calculated as in (1), which can be obtained by the most widely used geometries in the literature. When some of these parameters were not explicitly given, we give our best knowledge estimation. The information on the type of antenna polarization and the possibility to integrate with planar feeding lines is also given.

Vivaldi antennas have been proposed for wideband imaging applications [8], [9] as they are matched within a bandwidth of the order of several octaves and are able to provide stable beams over one octave [10]. Used in single feed per beam scenarios, Vivaldi antennas suffer from strong coupling [19]. Therefore, they are typically used as phased arrays for multiple feed per beam scenarios with F/D ratios typically less than 1 [8], [9].

Pyramidal and conical horns, common at high frequencies, are characterized by aperture efficiencies of about 50%–60% [32]–[35] and offer a bandwidth up to $1:1.5$. In order to achieve high reflector illumination efficiency, corrugated horn antennas have been proposed in the literature [11]–[16]. These antennas typically present low side lobe and cross-polarization levels. The aperture efficiencies of corrugated horns presented in [11] and [12] are comparable to the conventional ones as they are optimized for $2\lambda F/D$ feed spacing. The manufacturing difficulties are significant for corrugated horn-based FPAs at the millimeter and submillimeter frequencies. As an alternative solution, smooth-walled spline horn antennas have been proposed in [17] and [18]. Although such smooth-walled horns are typically characterized by slightly better aperture efficiencies compared with corrugated horns, they can only provide narrower operational bandwidth than corrugated ones due to their increased lengths.

Integrated lens antennas, on the other hand, can provide more practical solutions as they are easier to manufacture in tightly sampled FPAs [20]. A double slot antenna is the most widely used lens feed [21]. It provides an aperture efficiency of 75% at the center of the bandwidth. This is later limited to about $1:1.15$ by the impedance matching. Similar

designs have been investigated in [24], [26]. Wideband lens feeds such as the X-slot [22], [23], a broadband slot feed so-called XETS antenna [25], sinuous antenna [27], [28], and spiral antennas [29] have also been proposed in the literature. The X-slot antenna can operate over an octave bandwidth with aperture efficiency between 40% and 50% [23]. XETS antenna also provides an octave bandwidth with a linear polarization only [25]. A wideband and dual-polarized lens feed was proposed in [27]. The feed is based on a sinuous antenna with nearly frequency-independent patterns. Using the data provided in [27], we calculated the taper efficiencies at 12 and 24 GHz, to be 69% and 66%, respectively. Including a matching layer, this sinuous antenna will have a peak of about 50% aperture efficiency. When it comes to the feeding mechanism, either integrated or differential feeds can be used with sinuous antennas [27]. However, the use of planar feeds disturbs their radiation characteristics significantly [29], unless the width of the feeding lines is much smaller than the wavelength. A scaled version of the sinuous antenna presented in [28] was used to operate continuously within a frequency band starting from 60 up to 240 GHz. It is able to provide dual polarization with planar feeding lines. The width of the microstrip transmission lines used in [28] is about $\lambda_0/2000$, where λ_0 is free-space wavelength at the highest frequency in the design. The requirement of extremely small feeding lines limits the use of these antennas at higher frequencies.

Table I also includes the performance of our proposed design based on a leaky lens concept. The details of the antenna optimization are given in the following sections. The proposed dual-polarized leaky lens antenna provides a peak aperture efficiency of 70% and it is higher than 50% within a bandwidth of 1 : 5.25, while it exceeds 60% for a bandwidth of 1 : 2.5. Moreover, the proposed antenna does not suffer from significant coupling to the feeding lines affecting the radiation patterns as it has a much larger ground plane than the sinuous antenna. The microstrip width in the present design is about $1/86\lambda_0$ at the highest frequency. The design can be extended to coplanar waveguide feeding lines with a dimension of $1/39\lambda_0$ [37]. Based on these results, the proposed leaky antenna solution offers a viable path for tightly spaced and wideband integrated FPAs at high frequencies.

III. DUAL-POLARIZED LEAKY SLOT

The geometry of the proposed dual-polarized leaky slot antenna is sketched in Fig. 2. It consists of a semi-infinite dielectric with a permittivity of ϵ_r^{diel} fed by the leaky slot that is etched on a ground plane located on top of a membrane. The membrane is placed at a certain electrically small distance h from the bottom part of the lens. It has a permittivity of ϵ_r^{memb} and a thickness of h_m. On top of the membrane, two orthogonal long tapered slots are printed. The slots have a length of l_s, an initial width of w_0, and a final width of w_s. The orthogonal slots are coupled, in turn, by two orthogonal microstrips, of width w_m, printed on the other side of the membrane as shown in Fig. 2(c).

As the two slots are fed symmetrically, the performance of the two polarizations is the same. In order to generate
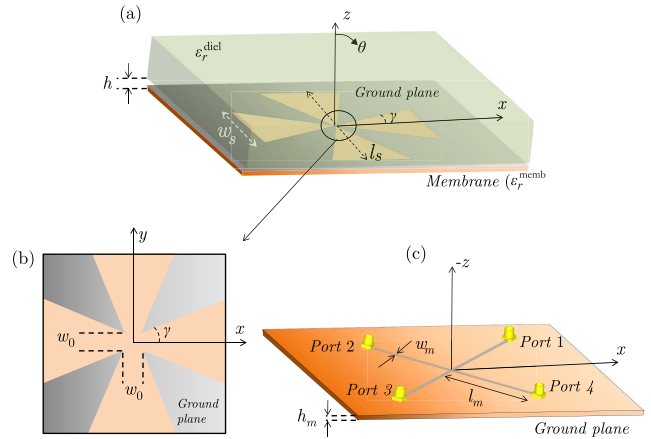

Fig. 2. Schematic of the microstrip fed dual-polarized leaky lens antenna. (a) Perspective view of the antenna with a semi-infinite silicon dielectric located on top, separated by an airgap, h, from the ground plane. (b) Central part of the crossing slots. (c) Microstrip transmission lines printed on the bottom side of the membrane to couple the radiation to the orthogonal slots.
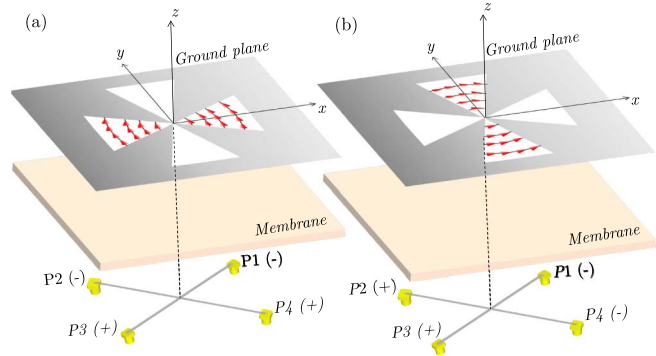

Fig. 3. Demonstration of the excitation mechanism of the dual-polarized leaky antenna depending on the port excitation signals.

the two polarizations, the microstrip transmission lines are fed by Port 1, Port 2, Port 3 and Port 4 simultaneously. Fig. 3 highlights the electric field distribution across the slots depending on the port excitations. To excite one polarization at a time, the ports should be fed using one of the following schemes:

1) Port 1 $= -V$, Port 2 $= -V$, Port 3 $= +V$ Port 4 $= +V$ (In order to excite the slot aligned along the x-axis).
2) Port 1 $= -V$, Port 2 $= +V$, Port 3 $= +V$ and Port 4 $= -V$ (In order to excite the slot aligned along the y-axis).

where V is the amplitude of voltage excitation defined for the ports in the simulations.

In the optimization process, we used a semi-infinite dielectric medium with a permittivity of $\epsilon_r^{\text{diel}} = 11.9$. In order to optimize the radiation patterns from the dual-polarized leaky slot, a parametric study is performed for a bandwidth of 1 : 2.5, starting from 8 to 20 GHz. In order to maximize the lens antenna aperture efficiency, for each of the polarizations, the leaky-wave slot should ideally generate a top hat pattern, inside the dielectric, with low cross-polarization. The shape of the pattern is directly related to the leaky-wave propagation
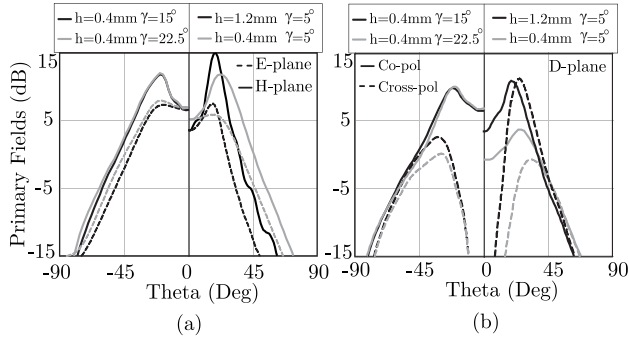
Fig. 4. Primary field variations inside the semi-infinite dielectric that is separated from the ground plane with an airgap h for various airgap and slot tapering angles, γ, at $f = 15$ GHz. (a) Includes co-polar beams in E and H-planes. (b) Highlights co- and cross-pol radiation in the D-plane.
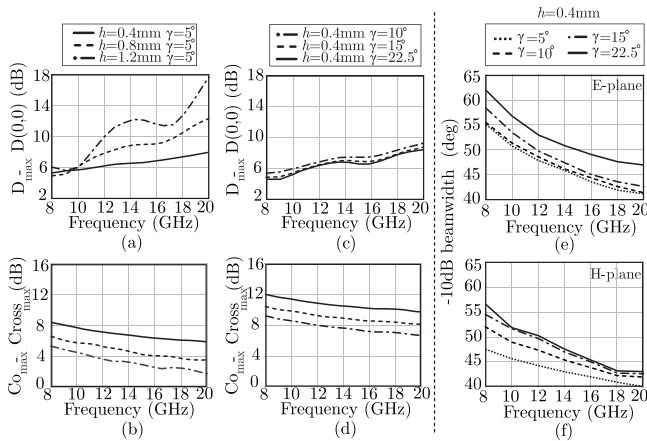

Fig. 5. Maximum directivity (D_{max}) with respect to broadside directivity ($D(0,0)$) as a function of (a) airgap distance, (b) tapering angle, and the difference between the maximum of co- and cross-polarizations for primary fields inside the semi-infinite dielectric for different (c) airgap values and (d) tapering angles. -10 dB beamwidth of the primary fields as a function of frequency is highlighted in (e) and (f) for E and H-planes, respectively.
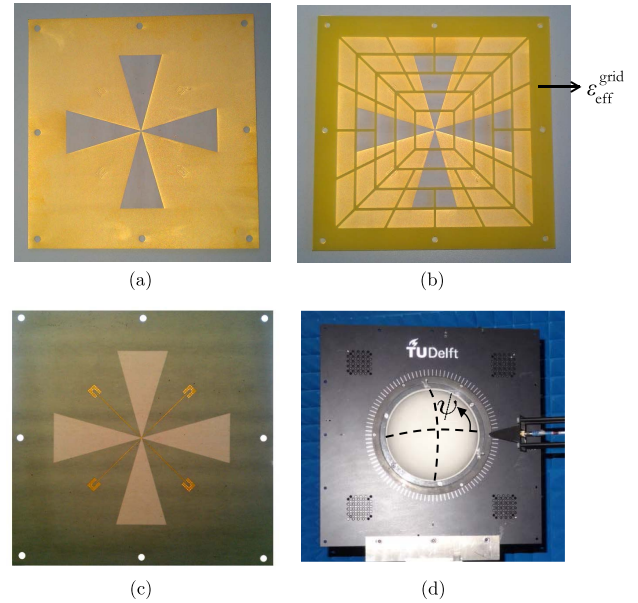

Fig. 6. Images of the low-frequency prototype. (a) Ground plane. (b) Ceramic grid located on top of the ground plane to serve as an airgap. (c) Microstrip feeding lines located underneath the membrane. (d) Dielectric lens located on top of the dual-polarized leaky-wave antenna.

constant, $\beta - j\alpha$ [30]. Typically, the pattern generated in silicon by a long slot in the presence of an air cavity has two pronounced peaks at $\theta = \pm \sin^{-1}(\beta/k_d)$, where k_d is the wavenumber in the silicon. Fig. 4 shows the radiated field inside the semi-infinite silicon dielectric medium simulated with CST MWS [38] at 15 GHz for various airgap and slot tapering angle values.

The leaky-wave propagation constant can be controlled by changing the height of the air cavity, h, and the width of the slot w_s. Larger cavity heights lead to leaky waves with smaller attenuation constants α. Fig. 5(a) shows the difference between the maximum directivity of the antenna (D_{max}) and the directivity at broadside ($D(0,0)$) as a function of the cavity height. Therefore the gap should be small, typically limited by the fabrication constraints. The cross-polarization level is instead influence by two parameters: the cavity height and the slot tapering angle. Fig. 5(b) shows the difference between the maximum level of the co- (Co_{max}) and cross-polarization ($Cross_{max}$) components as a function of the cavity height, whereas Fig. 5(c) and (d) shows the impact of the slot tapering angle. The larger the tapering angle, the lower the

cross-polarization level. The upper limit for the tapering angle is then given by a -10 dB beamwidth for proper lens illumination [21] and azimuthal symmetry of the radiated fields. The -10 dB beamwidth with respect to the broadside directivity, at various tapering angles, is highlighted in Fig. 5(e) and (f) for the E and H-planes, respectively. As a result, the optimum performance has been obtained for $h = 0.4$ mm, $w_0 = 0.24$ mm, and $w_s = 23$ mm, which corresponds to a slot tapering angle, γ, of about $15°$. The radiated pattern for these conditions is also shown in Fig. 4 and is representative of both dual- and single-polarized antennas.

IV. EXPERIMENTAL VALIDATION: RADIATION IN A SEMI-INFINITE DIELECTRIC

The dual-polarized slot has been manufactured using the standard printed technology and is shown in Fig. 6. The air cavity has been created using a grid structure of ceramic material of height $h = 0.4$ mm and permittivity of 3.55. Thanks to the gridded structure, the effective permittivity is close to $\epsilon_{eff}^{grid} = 1$. The membrane was made of Rogers RT6002 with a permittivity $\epsilon_r^{memb} = 2.94$ and a thickness of $h_m = 0.127$ mm. The transmission lines have a width of $w_m = 0.175$ mm and a length of $l_m = 30$ mm (From the connector to the center of the slot). The antenna presented is well matched to a microstrip line with a characteristic impedance of 60 Ω over a bandwidth larger than two octaves. The active reflection coefficient is measured and has good agreement with the CST simulations, as shown in Fig. 7.

In order to measure the radiated fields inside the dielectric, a near-field broadband waveguide probe operating from 9 to 26 GHz is located on top of a half dielectric sphere with a radius of $R = 95$ mm. The dielectric sphere is made of ECCOSTOCK HIK 500F [40], with a relative
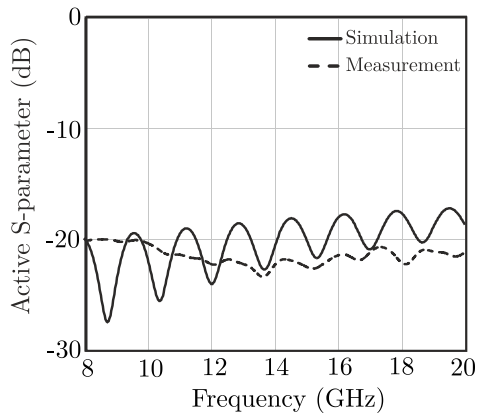
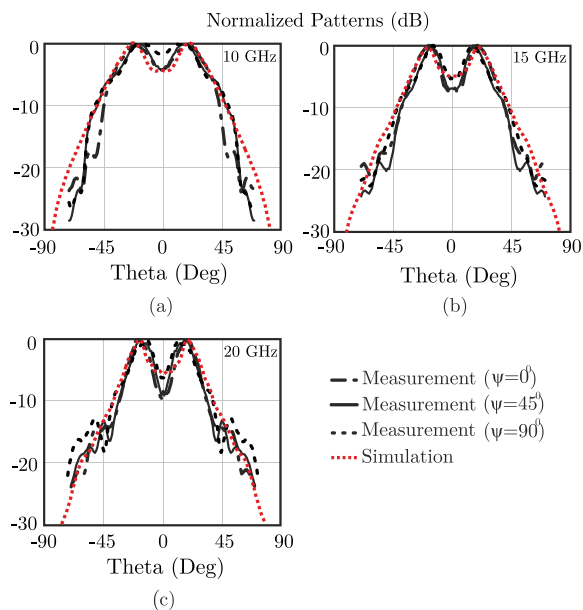Fig. 7. Comparison of the measured and simulated active S-parameters.

Fig. 8. Comparison of the H-plane measured patterns for three lens rotation angles, ψ, for frequencies at (a) 10, (b) 15, and (c) 20 GHz.

permittivity of 11.9. The antenna is fed by only one port at a time, while all the other ports are terminated with matched loads. The contributions from the other ports are taken into account by superposing the fields measured at each port. θ and ϕ-components of the field are measured by rotating the probe by 90° along its axis. The dielectric sphere is not covered by a matching layer and the inner reflections at the dielectric–air interface are time gated in postprocessing. During the measurement campaign, we found that the sphere material was not uniform and presents an anisotropic behavior. Therefore, the measurements were repeated thrice by rotating the dielectric sphere, only along ψ as shown in Fig. 6(d).

The measured radiated fields inside the dielectric are compared with the simulated ones at three frequencies, 10, 15 and 20 GHz in Figs. 8 and 9 for the H and E-plane, respectively. Due to the anisotropy, Figs. 8 and 9 include the measured fields at three different ψ sphere rotations. As it can be seen from the results, there is a good agreement between the measurements
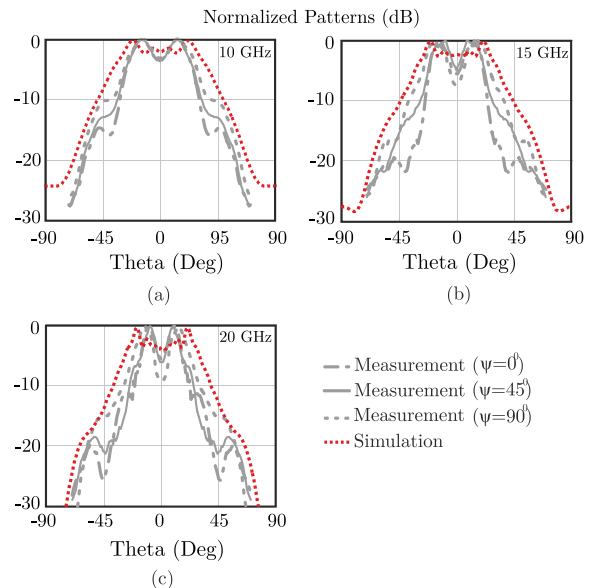

Fig. 9. Comparison of the E-plane measured patterns for three lens rotation angles, ψ, for frequencies at (a) 10, (b) 15, and (c) 20 GHz.

and CST simulations for H-plane whereas the agreement becomes worse for the E-plane. For this field polarization, the measured results depend strongly on the dielectric sphere rotation.

V. THz FPA Optimization

In this section, we present a practical implementation of a tightly packed FPA based on directive leaky lens feeds. The application of the proposed antenna is sub-mm astronomical observations with reflector systems of $F/D > 3$. For the lenses fed by directive feeds, the impact of the mutual coupling in the radiation pattern can be neglected. The lens antennas have been analyzed using a numerically efficient physical optics (PO) algorithm [39]. The schematic of the final lens geometry is shown in Fig. 1. The lens material has the same permittivity as the semi-infinite dielectric medium used for the slot optimization ($\epsilon_r^{\text{lens}} = \epsilon_r^{\text{diel}} = 11.9$) with having a radius of R, an aperture of D_f, an extension length of $L = 0.31R$, and a lens truncation angle of θ_{lens} (See Fig. 1). The lens is coated by a $\lambda_d/4$ matching layer made of Parylene material ($\epsilon_r^{\text{ML}} \approx 2.62$), where λ_d is the wavelength at inside the dielectric at the center frequency, f_0.

In Fig. 10 is shown the proposed leaky lens antenna aperture efficiency, η_{ap}, as a function of frequency. The lens antenna has a maximum aperture efficiency of about 70%, while it is higher than 60% within a bandwidth of about $1:2.5$. Moreover, it remains higher than 55% over the entire bandwidth (See Fig. 10). Here, the aperture efficiency is evaluated as

$$\eta_{\text{ap}}(f) = \eta_{\text{tap}}(f)\eta_{\text{feed}}(f) \quad (1)$$

where η_{feed} and η_{tap} refer to feed efficiency and lens taper efficiency, respectively. Taper efficiency is the ratio of the broadside directivity to the maximum directivity one can obtain using the same feed aperture size. Feed efficiency, on the other hand, is calculated as $\eta_{\text{feed}}(f) = \eta_{\text{ref}}(f)\eta_{\text{so}}(f)\eta z(f)$.
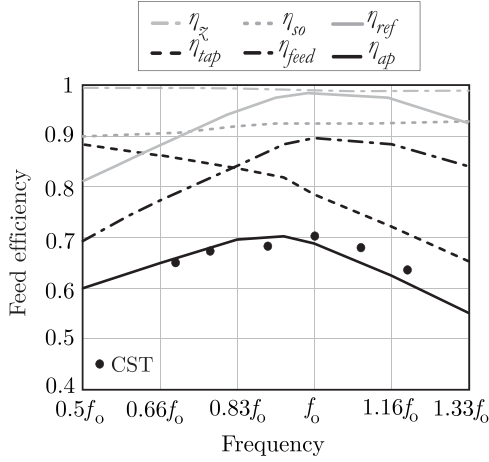
Fig. 10. Aperture efficiency of the proposed lens antenna as a function of frequency.

Fig. 11. Co and cross-pol radiation of the reflector feed with a lens aperture of $D_f = 10.66\lambda_0$ at frequencies of (a) $0.66f_0$ (b) f_0, and (c) $1.33f_0$, in the E, H, and D-planes. The region confined by the reflector subtended angle θ_0 corresponding to FPA feed separation of $d = \lambda_0 F/D$ is also highlighted together with the beams. Here (d) shows the Phase distribution of the secondary beams in E and H-planes at the same frequency points.

Here, η_{ref} refers to reflection efficiency due to the dielectric–air interface on the lens surface, η_z refers to the efficiency due to antenna impedance matching, and η_{so} refers to the spillover efficiency defined on the lens surface. The simulated aperture efficiencies obtained by full-wave CST simulations are also shown in Fig. 10 at six discrete frequency points (highlighted by black dots) obtaining good agreement between the PO and CST simulations.

As a specific example, here, we consider a proposed sub-millimeter wave space astronomical instrument envisioned to operate over an octave bandwidth from 1.4 to 2.7 THz and coupled to a telescope with $F/D > 10$ [2], [42]. Different feed samplings ($d = 0.5\lambda_0 F/D$, $d = \lambda_0 F/D$) of the focal plane are under consideration. Here λ_0 is the free-space wavelength at the center frequency, f_0. The proposed FPA design has a feed separation of $d = 1.6$ mm with the lenses having an aperture of $D_f = 1.6$ mm (which corresponds to $D_f = 10.66\lambda_0$), a radius of $R = 0.9$ mm (See Fig. 1), an extension length of $L = 0.31R$, and a lens truncation angle of $\theta_{lens} = 46.3°$.

The co- and cross-polar radiation patterns of the proposed lens antenna are shown in Fig. 11 for $0.66f_0$, f_0, and $1.33f_0$, respectively. Fig. 11 shows that the beams after the lens are quite symmetric in the E-, H-, and D-planes. The lens antenna has a cross-polarization less than -12 dB within an octave bandwidth. Phase distribution of the reflector feed patterns is shown in Fig. 11(d) for the E- and H-planes, at the same frequency points.

A. Reflector Simulations

In Fig. 12, we compare the reflector illumination efficiencies, simulated with GRASP, ($\eta_{tap}^{refl}\eta_{so}^{refl}\eta_{feed}$) obtained by the proposed design and a feed with a uniform aperture current distribution ($\eta_{ap} = 100\%$) for $d = 0.5, 1$, and $2\lambda_0 F/D$ feed spacings as a function of frequency. The ratio of the reflector efficiencies ($\eta_{leaky}/\eta_{uniform}$) for feed samplings $d \leq \lambda_0 F/D$ is basically the feed aperture efficiency shown in Fig. 10. This is because the reflector illumination efficiency is solely dominated by the reflector spillover efficiency for tightly
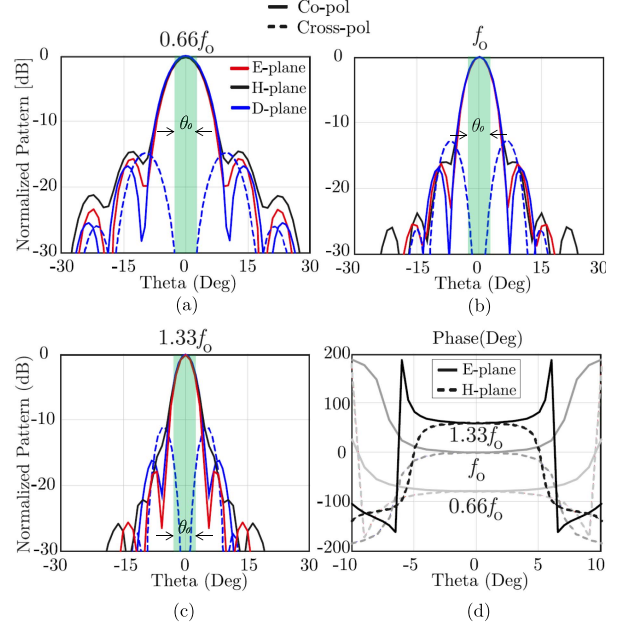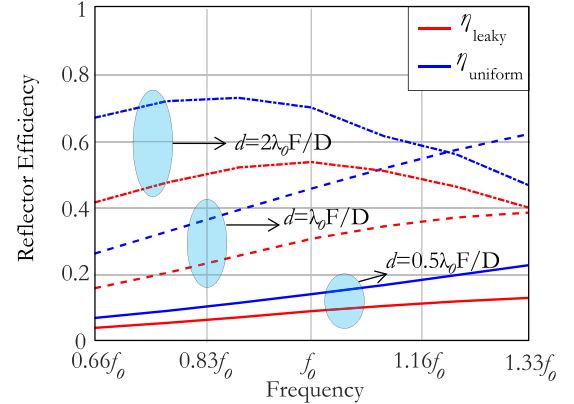

Fig. 12. Reflector efficiency comparisons (including the feed efficiency, η_{feed}) between the proposed leaky slot and an ideal uniformly excited feed for different feed separations d in the FPA as a function of frequency.

spaced FPAs ($d \leq \lambda_0 F/D$). Therefore, for such small feed samplings, one has to maximize the feed taper efficiency. Instead, for $d = 2\lambda_0 F/D$, the reflector efficiency is a tradeoff between spillover and taper efficiencies, and therefore the reflector feeds are typically optimized for high Gaussicity [21].

The radiated patterns from the considered telescope are shown in Fig. 13 for $d = 0.5\lambda_0 F/D$ and $\lambda_0 F/D$. The $2\lambda_0 F/D$ is also included in Fig. 13 for reference. It shows that tight samplings lead to lower cross-polarization levels in the telescope radiation patterns as the feed cross-polarized fields do not reach the telescope (i.e., smaller subtended angle, θ_0, as shown in Fig. 11). Therefore, for tightly spaced FPAs, the achieved cross-polarization level in the proposed antenna system is less than -35 dB.
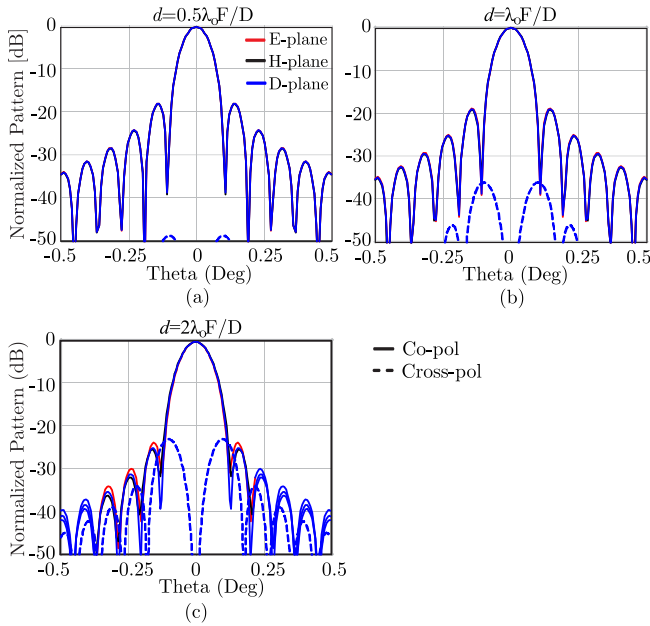
Fig. 13. Co and cross-pol components of the reflector patterns obtained by the proposed lens antenna design with a fixed aperture diameter of $D_f = 10.66\lambda_0$ for three feed samplings: (a) $d = 0.5\lambda_0 F/D$, (b) $d = \lambda_0 F/D$, and (c) $d = 2\lambda_0 F/D$.

VI. CONCLUSION

The dual-polarized leaky lens antenna presented in this paper is able to provide clean symmetric beams with high aperture efficiencies for a bandwidth of more than one octave. The proposed antenna provides a planar integrated solution that allows an easy and low-cost manufacturing process unlike the horn antenna solutions, as they suffer from these issues, especially for higher millimeter and submillimeter wavelengths. The design has a maximum lens aperture efficiency of 70%, while it operates within a bandwidth of over $1 : 5$ with an aperture efficiency of more than 50% or $1 : 2.5$, where the aperture efficiency is more than 60%. The entire antenna system has a very good cross-polarization performance. Namely, the maximum cross-polarization level is less than -35 dB for $d = \lambda_0 \ F$ sampling, whereas it remains even lower, less than -49 dB, for $d = 0.5\lambda_0 \ F$. Based on the results highlighted in this paper, we believe that the proposed antenna design lends itself as an extremely useful alternative for next-generation submillimeter wave space astronomical instruments.

REFERENCES

[1] A. Baryshev *et al.*, "Progress in antenna coupled kinetic inductance detectors," *IEEE Trans. THz Sci. Technol.*, vol. 1, no. 1, pp. 112–123, Sep. 2011.

[2] A. Neto, N. Llombart, B. Blázquez, and A. Freni, "Imaging speed of antenna coupled kinetic inductance detectors in the SAFARI/SPICA scenario," in *Proc. 8th Eur. Conf. Antennas Propag.*, The Hague, The Netherlands, Apr. 2014, pp. 3524–3525.

[3] A. Akgiray, S. Weinreb, W. A. Imbriale, and C. Beaudoin, "Circular quadruple-ridged flared horn achieving near-constant beamwidth over multioctave bandwidth: Design and measurements," *IEEE Trans. Antennas Propag.*, vol. 61, no. 3, pp. 1099–1108, Mar. 2013.

[4] R. Olsson, P.-S. Kildal, and S. Weinreb, "The eleven antenna: A compact low-profile decade bandwidth dual polarized feed for reflector antennas," *IEEE Trans. Antennas Propag.*, vol. 54, no. 2, pp. 368–375, Feb. 2006.

[5] O. Yurduseven, D. Cavallo, and A. Neto, "Wideband dielectric lens antenna with stable radiation patterns fed by coherent array of connected leaky slots," *IEEE Trans. Antennas Propag.*, vol. 62, no. 4, pp. 1895–1902, Apr. 2014.

[6] C. A. Fernandes, E. B. Lima, and J. R. Costa, "Broadband integrated lens for illuminating reflector antenna with constant aperture efficiency," *IEEE Trans. Antennas Propag.*, vol. 58, no. 12, pp. 3805–3813, Dec. 2010.

[7] N. T. Nguyen, A. V. Boriskin, A. Rolland, L. Le Coq, and R. Sauleau, "Shaped lens-like dome for UWB antennas with a Gaussian-like radiation pattern," *IEEE Trans. Antennas Propag.*, vol. 61, no. 4, pp. 1658–1664, Apr. 2013.

[8] M. V. Ivashina, J. D. Bregman, J. G. B. de Vaate, L. Li, and A. J. Parfitt, "Experimental results for a focal plane array, synthesized with conjugate field method," in *Proc. Int. Symp. Antennas Propag. Soc.*, Jun. 2004, pp. 21–24.

[9] D. H. Schaubert, E. L. Kollberg, T. Korzeniowski, T. Thungren, J. Johansson, and K. S. Yngvesson, "Endfire tapered slot antennas on dielectric substrates," *IEEE Trans. Antennas Propag.*, vol. 33, no. 12, pp. 1392–1400, Dec. 1985.

[10] P. J. Gibson, "The Vivaldi Aerial," in *Proc. 9th Eur. Microw. Conf.*, Sep. 1979, pp. 101–105.

[11] J. Teniente, R. Gonzalo, and C. del-Río, "Ultra-wide band corrugated Gaussian profiled horn antenna design," *IEEE Microw. Wireless Compon. Lett.*, vol. 12, no. 1, pp. 20–21, Jan. 2002.

[12] J. C. S. Chieh, B. Dick, S. Loui, and J. D. Rockway, "Development of a Ku-band corrugated conical horn using 3-D print technology," *IEEE Antennas Wireless Propag. Lett.*, vol. 13, pp. 201–204, Feb. 2014.

[13] S. Sekiguchi *et al.*, "Direct machined broadband corrugated horn array for millimeter observations," in *Proc. 16th Int. Workshop Low Temperature Detect.*, Grenoble, France, Jul. 2015.

[14] M. M. Kangas *et al.*, "A 31 pixel flared 100-GHz high-gain scalar corrugated nonbonded platelet antenna array," *IEEE Antennas Wireless Propag. Lett.*, vol. 4, pp. 245–248, 2005, doi: 10.1109/LAWP.2005.852578.

[15] J. W. Britton *et al.*, "Corrugated silicon platelet feed horn array for CMB polarimetry at 150 GHz," *Proc. SPIE*, vol. 7741, pp. 77410T-1–77410T-11, 2010, doi: 10.1117/12.857701.

[16] J. P. Nibarger *et al.*, "An 84 pixel all-silicon corrugated feedhorn for CMB measurements," *J. Low Temperature Phys.*, vol. 167, nos. 3–4, pp. 522–527, Jan. 2012.

[17] A. Hammar, Y. Karandikar, P. Forsberg, A. Emrich, and J. Stake, "A 340 GHz high Gaussicity smooth spline horn antenna for the STEAMR instrument," in *Proc. IEEE Antennas Propag. Soc. Int. Symp.*, Memphis, TN, USA, Jul. 2014, pp. 649–650.

[18] C. Granet, G. L. James, R. Bolton, and G. Moorey, "A smooth-walled spline-profile horn as an alternative to the corrugated horn for wide band millimeter-wave applications," *IEEE Trans. Antennas Propag.*, vol. 52, no. 3, pp. 848–854, Mar. 2004.

[19] J. Johansson, "Tapered slot antennas and focal plane imaging systems," Ph.D. dissertation, School Elect. Comput. Eng., Chalmers Univ. Technol., Gothenburg, Sweden, 1988.

[20] A. M. Baryshev *et al.*, "Large format antenna coupled micorwave kinetic iinductance detector arrays for radioastronomy," in *Proc. Int. Conf. Infr., Millim., Terahertz Waves*, Tucson, AZ, USA, Sep. 2014.

[21] D. F. Filipovic, S. S. Gearhart, and G. M. Rebeiz, "Double-slot antennas on extended hemispherical and elliptical silicon dielectric lenses," *IEEE Trans. Microw. Theory Techn.*, vol. 41, no. 10, pp. 1738–1749, Oct. 1993.

[22] A. Iacono, T. J. Coenen, D. J. Bekers, A. Neto, and G. Gerini, "Trade-offs in multi-element receiving antennas with superconducting feed lines," in *Proc. 4th Eur. Conf. Antennas Propag.*, Barcelona, Spain, Apr. 2010, pp. 1–5.

[23] P. J. de Visser, J. J. A. Baselmans, J. Bueno, N. Llombart, and T. M. Klapwijk, "Fluctuations in the electron system of a superconductor exposed to a photon flux," *Nature Commun.*, vol. 5, Feb. 2013, Art. no. 3130, doi: 10.1038/ncomms4130.

[24] G. C. Trichopoulos, H. L. Mosbacker, D. Burdette, and K. Sertel, "A broadband focal plane array camera for real-time THz imaging applications," *IEEE Trans. Antennas Propag.*, vol. 61, no. 4, pp. 1733–1740, Apr. 2013.

[25] J. R. Costa and C. A. Fernandes, "Broadband slot feed for integrated lens antennas," *IEEE Antennas Wireless Propag. Lett.*, vol. 6, pp. 396–400, Aug. 2007.

[26] A. D. Semenov *et al.*, "Terahertz performance of integrated lens antennas with a hot-electron bolometer," *IEEE Trans. Microw. Theory Techn.*, vol. 55, no. 2, pp. 239–247, Feb. 2007.

[27] J. M. Edwards, R. O'Brient, A. T. Lee, and G. M. Rebeiz, "Dual-polarized sinuous antennas on extended hemispherical silicon lenses," *IEEE Trans. Antennas Propag.*, vol. 60, no. 9, pp. 4082–4091, Sep. 2012.

[28] R. O'Brient *et al.*, "A Dual-polarized broadband planar antenna and channelizing filter bank for millimeter wavelengths," *Appl. Phys. Lett.*, vol. 102, no. 6, p. 063506, Feb. 2013, doi: 10.1063/1.4791692.

[29] A. Garufo, N. Llombart, and A. Neto, "Demonstration of the enhanced radiation in dielectric lens spiral antennas," in *Proc. 8th Eur. Conf. Antennas Propag.*, The Hague, The Netherlands, Apr. 2014.

[30] A. Neto, "UWB, non dispersive radiation from the planarly fed leaky lens antenna—Part 1: Theory and design," *IEEE Trans. Antennas Propag.*, vol. 58, no. 7, pp. 2238–2247, Jul. 2010.

[31] A. Neto, N. Llombart, J. J. A. Baselmans, A. Baryshev, and S. J. C. Yates, "Demonstration of the leaky lens antenna at submillimeter wavelengths," *IEEE Trans. Terahertz Sci. Technol.*, vol. 4, no. 1, pp. 26–32, Jan. 2014.

[32] *Datasheet Provided by Farview Microwave*, accessed on 2016. [Online]. Available: http://www.fairviewmicrowave.com/images/product PDF/SH190-20.pdf

[33] Y. T. Lo and S. W. Lee, *Antenna Handbook: Theory, Applications, and Design*. New York, NY, USA: Van Nostrand, 1988.

[34] C. A. Balanis, *Antenna Theory: Analysis and Design*, 3rd ed. Hoboken, NJ, USA: Wiley, 2005.

[35] R. C. Johnson and H. Jasik, *Antenna Engineering Handbook*, 2nd ed. New York, NY, USA: McGraw-Hill, 1984.

[36] J. Gao *et al.*, "A semiempirical model for two-level system noise in superconducting microresonators," *Appl. Phys. Lett.*, vol. 92, no. 21, p. 212504, May 2008, doi: 10.1063/1.2937855.

[37] N. Llombart, O. Yurduseven, A. Neto, I. E. Lager, and J. Baselmans, "Dual polarised antenna for THz space applications: Design and optimization," in *Proc. 44th Eur. Microw. Conf.*, Rome, Italy, Oct. 2014, pp. 100–103, doi: 10.1109/EuMC.2014.6986379.

[38] *The Homepage of CST Microwave Studio*, accessed on 2016. [Online]. Available: http://www.cst.com/

[39] M. Albani, G. Carluccio, and P. H. Pathak, "Uniform ray description for the PO scattering by vertices in curved surface with curvilinear edges and relatively general boundary conditions," *IEEE Trans. Antennas Propag.*, vol. 59, no. 5, pp. 1587–1596, May 2011.

[40] *The homepage of Emerson & Cuming MicroWave Products*. [Online]. Available: http://www.eccosorb.eu/

[41] *The homepage of SPACEKIDs Project*. [Online]. Available: http://www.spacekids.eu/index.php

[42] P. Roelfsema *et al.*, "The SAFARI imaging spectrometer for the SPICA space observatory," *Proc. SPIE.*, vol. 8442, pp. 84420R-1–84420R-15, Sep. 2012, doi: 10.1117/12.927010.

Nuria Llombart Juan (S'06–M'07–SM'13) received the Electrical Engineering and Ph.D. degrees from the Polytechnic University of Valencia, Valencia, Spain, in 2002 and 2006, respectively.

She spent one year with the Friedrich-Alexander University of Erlangen-Nuremberg, Erlangen, Germany, and was with the Fraunhofer Institute for Integrated Circuits, Erlangen, during her master's studies. From 2002 to 2007, she was with the Antenna Group, TNO Defence, Security and Safety Institute, The Hague, The Netherlands, as a Researcher. From 2007 to 2010, she was a Post-Doctoral Fellow with the Sub-Millimeter Wave Advance Technology Group, Jet Propulsion Laboratory, California Institute of Technology, Pasadena, CA, USA. She was a Ramn y Cajal Fellow with the Optics Department, Complutense University of Madrid, Madrid, Spain, from 2010 to 2012. In 2012, she joined the THz Sensing Group, Delft University of Technology, Delft, The Netherlands, where she is currently an Associate Professor. She has co-authored over 100 journal and international conference contributions. Her current research interests include the analysis and design of planar antennas, periodic structures, reflector antennas, lens antennas, and waveguide structures, with an emphasis on the THz range.

Dr. Llombart Juan was a co-recipient of the H. A. Wheeler Award for the Best Applications Paper in the IEEE TRANSACTIONS ON ANTENNAS AND PROPAGATION in 2008, the 2014 THz Science and Technology Best Paper Award of the IEEE Microwave Theory and Techniques Society, and several NASA awards. She received the 2014 IEEE Antenna and Propagation Society Lot Shafai Mid-Career Distinguished Achievement Award. She serves as a Topical Editor of the IEEE TRANSACTIONS ON TERAHERTZ SCIENCE AND TECHNOLOGY, the IEEE ANTENNAS AND WIRELESS PROPAGATION LETTERS, and the Antenna Applications Corner of the *EEE Antennas and Propagation Magazine*. She is also a Board Member of the IRMMW-THz International Society.

Ozan Yurduseven (S'11) received the B.Sc. and M.Sc. (Hons.) degrees in electronics and communications engineering from Yıldız Technical University, Istanbul, Turkey, in 2009 and 2011, respectively. He is currently pursuing the Ph.D. degree with the Electrical Engineering, Mathematics and Computer Science Department, Delft University of Technology, Delft, The Netherlands.

He was a Research Assistant with the Electromagnetics Department, Ankara University, Ankara, Turkey, from 2010 to 2012. During his Ph.D. research, he spent six months with the Instituto de Telecomunicações, Instituto Superior Técnico, Lisbon, Portugal, where he was involved in the dielectric lens antenna design for THz imaging systems. He has authored or co-authored over 30 publications in peer-reviewed journals and conferences. His current research interests include millimeter and sub-millimeter wave antenna design, dielectric lens antennas for THz imaging applications, numerical techniques in electromagnetics, radar cross section analysis, and metamaterials.

Mr. Yurduseven is a member of the IEEE Antennas and Propagation Society and the European Association on Antennas and Propagation. He received the Best Student Paper Prize at the European Conference on Antennas and Propagation in 2013. He serves as a Reviewer of the IEEE TRANSACTIONS ON ANTENNAS AND PROPAGATION, the IEEE ANTENNAS AND WIRELESS PROPAGATION LETTERS, and *IET Microwaves, Antennas and Propagation*.

Andrea Neto (M'00–SM'10–F'16) received the Laurea (*summa cum laude*) degree in electronics engineering from the University of Florence, Florence, Italy, in 1994, and the Ph.D. degree in electromagnetics from the University of Siena, Siena, Italy, in 2000.

Part of his Ph.D. was developed with the European Space Agency Research and Technology Center, Noordwijk, The Netherlands, where he was with the Antenna Section for over two years. From 2000 to 2001, he was a Post-Doctoral Researcher with the Sub-Millimeter Wave Advanced Technology Group, California Institute of Technology, Pasadena, CA, USA. From 2002 to 2010, he was a Senior Antenna Scientist with TNO Defence, Security and Safety, The Hague, The Netherlands. In 2010, he was appointed as a Full Professor of Applied Electromagnetism with the Electrical Engineering, Mathematics and Computer Science Department, Delft University of Technology, Delft, The Netherlands, where he formed and currently leads the THz Sensing Group. His current research interests include the analysis and design of antennas, with an emphasis on arrays, dielectric lens antennas, wideband antennas, EBG structures, and THz antennas.

Dr. Neto is a member of the Technical Board of the European School of Antennas and an Organizer of the course on Antenna Imaging Techniques. He is a member of the Steering Committee of the Network of Excellence NEWFOCUS, dedicated to focusing techniques in millimeter and sub-millimeter wave regimes. He was a co-recipient of the H. A. Wheeler Award for the Best Applications Paper in the IEEE TRANSACTIONS ON ANTENNAS AND PROPAGATION in 2008, the Best Innovative Paper Prize at the 30th ESA Antenna Workshop in 2008, and the Best Antenna Theory Paper Prize at the European Conference on Antennas and Propagation in 2010. In 2011, he received a five years starting grant from the European Research Council for Advanced THz Antennas. He serves as an Associate Editor of the IEEE TRANSACTIONS ON ANTENNAS AND PROPAGATION and the IEEE ANTENNAS AND WIRELESS PROPAGATION LETTERS. He served as an Associate Editor of the IEEE TRANSACTIONS ON ANTENNAS AND PROPAGATION from 2008 to 2013, and the IEEE ANTENNAS AND WIRELESS PROPAGATION LETTERS from 2005 to 2013.